

A finite-difference scheme for mixed boundary value problems of arbitrary-shaped elastic bodies

M. Abdus Salam Akanda^a, S. Reaz Ahmed^a, M. Raisuddin Khan^b, M. Wahhaj Uddin^{a,*}

^aDepartment of Mechanical Engineering, Bangladesh University of Engineering and Technology, Dhaka -1000, Bangladesh

^bDepartment of Mechanical Engineering, Bangladesh Institute of Technology, Chittagong, Bangladesh

Received 16 February 1998; received in revised form 9 April 1999; accepted 6 July 1999

Abstract

This paper presents a program based on a finite-difference technique, which solves plane stress and plane strain problems of arbitrary shaped elastic bodies with mixed boundary conditions. A new formulation of governing equations in terms of the displacement potential function ψ , as introduced by Uddin (Finite difference solution of two-dimensional elastic problems with mixed boundary conditions, MSc Thesis, Carleton University, Canada, 1966), has been used. This formulation has the capability to handle problems of mixed boundary condition, which is beyond the ability of the conventional formulations in terms of Airy's stress function ϕ . Results found with this program for classical problems are in very good agreement with known solutions. This program can handle practical boundary conditions very efficiently. © 2000 Elsevier Science Ltd. All rights reserved.

Keywords: Finite-difference scheme; Airy's stress function; Arbitrary-shaped elastic bodies

Nomenclature

| | |
|------------|--|
| E | elastic modulus of the material |
| a, b | addendum and dedendum of gear tooth |
| c, d | half depth and length of the deep cantilever and simply supported beam |
| h, k | mesh lengths in the x - and y -directions |
| i, j | grid positions with reference to x - and y -coordinates |
| l, m | direction cosines of the normal at any point on the boundary |
| m_o, d_p | module, pitch diameter of gear |
| n_1, n_2 | number of grids in the x - and y -directions |
| q | specific weight of the liquid |
| t | width of a simply supported beam |
| u, v | displacement components in the x - and y -directions |
| u_n, u_t | normal and tangential displacement components on the physical boundary |
| w | uniformly distributed loading on simply supported beam |
| x, y | rectangular coordinates |

| | |
|---|---|
| σ_n, σ_t | normal and tangential stress components on the physical boundary |
| $\sigma_x, \sigma_y, \sigma_{xy}$ | stress components in the x -direction, y -direction and xy -plane |
| ϕ | Airy's stress function |
| ψ | potential function defined in terms of displacement components |
| θ_p | pressure angle of gear tooth |
| μ | Poisson's ratio |
| $\bar{\sigma}_n, \bar{\sigma}_t$ | $\sigma_n/E, \sigma_t/E$ |
| $\bar{\sigma}_x, \bar{\sigma}_y, \bar{\sigma}_{xy}$ | $\sigma_x/E, \sigma_y/E, \sigma_{xy}/E$ |

1. Introduction

Elasticity is now a classical subject and its problems are even more classical. But somehow these stress analysis problems are still suffering from a lot of shortcomings and thus are being constantly looked into [1–13]. We have often failed in establishing a very good correlation between analyses and observation. To make-up this lack of good correlation, we have conjectured the behavior of materials in terms of its ultimate strength, yield strength, endurance strength, fracture strength, but still could not really satisfactorily account for the shortcomings. Two factors may really be responsible for it. Both these factors involve management of the boundary of elastic problems: one is the condition

* Corresponding author. Tel.: + 880-2-966-1756; fax: + 880-2-863-046.

E-mail address: wahhaj@me.buet.edu (M. Wahhaj Uddin).

and the other is the boundary shape. The necessity of the management of boundary shape has led to the invention of the finite element technique and its overwhelming popularity, specifically because of the side by side development of high-powered computing machines. Of course, the adaptations of the finite-element method relieved us from our major inability of managing odd boundary shapes but we are constantly aware of its lack of sophistication and doubtful quality of the solutions so obtained. The other factor of impediment to quality solutions of elastic problems is the treatment of the transition in boundary conditions. Elastic problems are either formulated in terms of deformation parameters or stress parameters. But, at the boundary, all the problems are invariably subjected to the mixture of both known deformations and known stress parameters. But neither of the two formulations would allow us to account fully both these two types of boundary conditions with equal sophistication in the region of transition where boundary conditions change from one type to the other.

This paper is an attempt to overcome both these two difficulties faced in the management of boundaries. It uses a new formulation of two-dimensional elastic problems, which enables us to manage the mixed mode in the boundary conditions as well as the zones of their transition. The computational work in this formulation is of the same magnitude as in the stress formulation, in case of numerical approach of solutions. The difficulties of boundary shapes for which the finite element method of solution of elastic problems was invented with a manifold increase of computational works and a lot of loss in sophistication is substituted by an innovative technique in the management of boundary shapes in the finite difference method of solutions.

The formulation of two-dimensional elastic problems used here was first introduced by Uddin in Ref. [8], later Idris used it in Ref. [10] for obtaining analytical solutions of a number of mixed boundary-value elastic problems, and Ahmed extended its use in Refs. [11,12] where he obtained finite-difference solutions of a number of mixed boundary value problems of simple boundary shapes. This paper simply extends the earlier works to include the problems of arbitrary boundary shapes. The rationality and the reliability of the formulation is thus checked repeatedly by comparing the results of mixed boundary value elastic problems obtained through this formulation with those available in the literature.

The formulation of two-dimensional elastic problems as used in this paper is in terms of a displacement potential function ψ , which has to satisfy the bi-harmonic differential equation like the Airy's stress function ϕ [7]. Thus the computational works in solving any problem remain the same in this case as it was in the case of Airy's stress function ϕ .

2. Governing equations in terms of displacement potential function, Ψ

Analysis of stresses in a material body is usually a three-dimensional problem. Fortunately, in most cases, the stress analysis of three-dimensional bodies can easily be treated as a two-dimensional problem, because most of the practical problems are often found to conform to the states of plane stress or plane strain. In the case of the absence of any body forces, the equations governing the three stress components σ_x , σ_y and σ_{xy} under the states of plane stress or plane strain are:

$$\frac{\partial \sigma_x}{\partial x} + \frac{\partial \sigma_{xy}}{\partial y} = 0 \quad (1)$$

$$\frac{\partial \sigma_y}{\partial y} + \frac{\partial \sigma_{xy}}{\partial x} = 0 \quad (2)$$

$$\left(\frac{\partial^2}{\partial x^2} + \frac{\partial^2}{\partial y^2} \right) (\sigma_x + \sigma_y) = 0 \quad (3)$$

Replacement of the stress components in Eqs. (1)–(3) by their relations with the displacement components u and v makes Eq. (3) redundant and transforms Eqs. (1) and (2) to

$$\frac{\partial^2 u}{\partial x^2} + \left(\frac{1 - \mu}{2} \right) \frac{\partial^2 u}{\partial y^2} + \left(\frac{1 + \mu}{2} \right) \frac{\partial^2 v}{\partial x \partial y} = 0 \quad (4)$$

$$\frac{\partial^2 v}{\partial y^2} + \left(\frac{1 - \mu}{2} \right) \frac{\partial^2 v}{\partial x^2} + \left(\frac{1 + \mu}{2} \right) \frac{\partial^2 u}{\partial x \partial y} = 0 \quad (5)$$

The problem thus reduces to finding u and v in a two-dimensional field satisfying the two elliptic partial differential equations (4) and (5).

In this paper, the problem is reduced to the determination of a single function instead of two functions u and v , simultaneously, satisfying the equilibrium equations (4) and (5). In this formulation, as in the case of Airy's stress function ϕ [7], a potential function $\psi(x, y)$ is defined in terms of displacement components as

$$\begin{cases} u = \frac{\partial^2 \psi}{\partial x \partial y} \\ v = -\frac{1}{1 + \mu} \left[(1 - \mu) \frac{\partial^2 \psi}{\partial y^2} + 2 \frac{\partial^2 \psi}{\partial x^2} \right] \end{cases} \quad (6)$$

When the displacement components in Eqs. (4) and (5) are replaced by $\psi(x, y)$, Eq. (4) is automatically satisfied and the only condition that ψ has to satisfy becomes

$$\frac{\partial^4 \psi}{\partial x^4} + 2 \frac{\partial^4 \psi}{\partial x^2 \partial y^2} + \frac{\partial^4 \psi}{\partial y^4} = 0 \quad (7)$$

Therefore, the problem is now formulated in such a way that a single function ψ has to be evaluated from the bi-harmonic equation (7), satisfying the boundary conditions that are specified at the boundary.

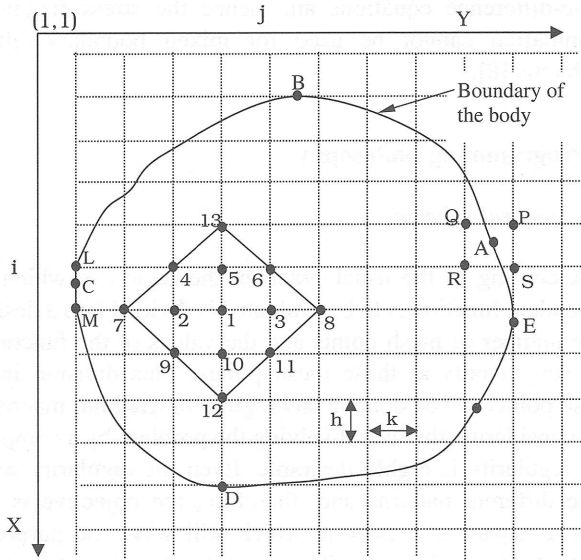


Fig. 1. Arbitrary-shaped body in a rectangular-grid field.

3. Boundary condition with Ψ -formulation

The boundary conditions at any point on an arbitrary-shaped boundary are known in terms of the normal and tangential components of displacement, u_n and u_t , and of stress, σ_n , and σ_t . These four components are expressed in terms of $\sigma_x, \sigma_y, \sigma_{xy}, u, v$ —the components of stress and displacement with respect to the reference axes x and y of the body, as follows:

$$u_n = u.l + v.m \tag{8}$$

$$u_t = v.l - u.m \tag{9}$$

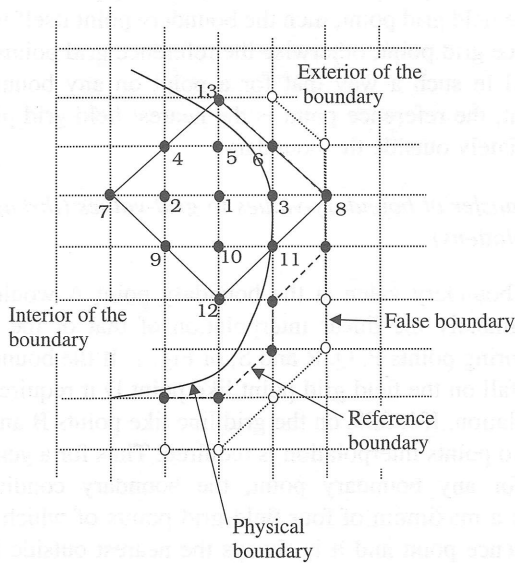


Fig. 2. Discretization of the governing equation at points in the immediate neighborhood of the physical boundary.

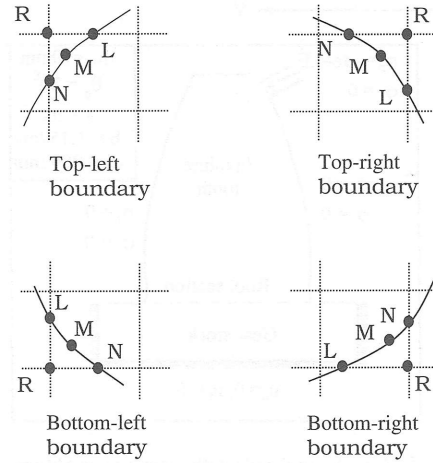


Fig. 3. Reference grid point R corresponding to boundary points L, M & N on the boundary segment LN.

$$\sigma_n = \sigma_x.l^2 + 2.\sigma_{xy}.l.m. + \sigma_y.m^2 \tag{10}$$

$$\sigma_t = (l^2 - m^2)\sigma_{xy} + l.m(\sigma_y - \sigma_x) \tag{11}$$

Here, l and m are the direction cosines of the normal to the boundary. The boundary conditions at any point on the boundary are specified in terms of any two known values of u_n, u_t, σ_n , and σ_t .

In order to solve the mixed boundary-value problems of irregular-shaped bodies using the present formulation, the boundary conditions need to be expressed in terms of ψ (which can be done by substituting the following expressions of the components of displacement and stress with respect to the reference axes x and y in terms of ψ in Eqs. (8)–(11).

$$u(x, y) = \frac{\partial^2 \psi}{\partial x \partial y} \tag{12}$$

$$v(x, y) = -\frac{1}{1 + \mu} \left[(1 - \mu) \frac{\partial^2 \psi}{\partial y^2} + 2 \frac{\partial^2 \psi}{\partial x^2} \right] \tag{13}$$

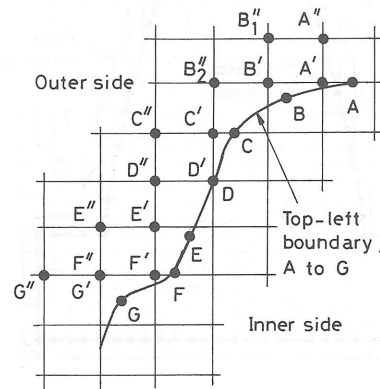


Fig. 4. Actual boundary points on the physical boundary and their corresponding reference points with extra field grid points.

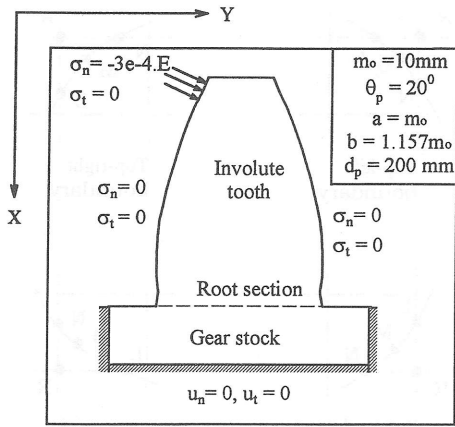


Fig. 5. Gear tooth details with boundary conditions.

$$\sigma_x(x, y) = \frac{E}{(1 + \mu)^2} \left[\frac{\partial^3 \psi}{\partial x^2 \partial y} - \mu \frac{\partial^3 \psi}{\partial y^3} \right] \quad (14)$$

$$\sigma_y(x, y) = -\frac{E}{(1 + \mu)^2} \left[\frac{\partial^3 \psi}{\partial y^3} + (2 + \mu) \frac{\partial^3 \psi}{\partial x^2 \partial y} \right] \quad (15)$$

$$\sigma_{xy}(x, y) = \frac{E}{(1 + \mu)^2} \left[\mu \frac{\partial^3 \psi}{\partial x \partial y^2} - \frac{\partial^3 \psi}{\partial x^3} \right] \quad (16)$$

As far as numerical method of solution of Eq. (7) is concerned, it is evident from the expressions of boundary conditions (8)–(11) that, no matter what combinations of two conditions are specified on the boundary, the whole range of conditions that ψ has to satisfy Eq. (7) within the body and any two of the Eqs. (8)–(11) at points on the boundary) can be expressed as finite-difference equations in terms of $\psi(x, y)$. Here, it should be pointed that, in case of Airy's stress function, the boundary conditions known in terms of displacement components cannot be expressed in

finite-difference equations and hence the stress function formulation cannot be used for mixed boundary-value problems [8].

4. Programming philosophy

4.1. General scheme

According to the usual practice, the region in which a dependent function is to be evaluated is divided into a desirable number of mesh points and the values of the function are sought only at these mesh points. This division into mesh points can be done in any regular or irregular manner, but considering the fact of solving the problem by a computer, regularity is highly desirable. Even the regularity will have different patterns and, therefore, the objective is to choose a particular pattern, which will serve the purpose in the best possible way. The present program is to solve a function within a geometrically irregular region, which is divided into meshes with lines parallel to rectangular coordinate axes. As a result, the boundary may not pass through the rectangular mesh points, as shown in Fig. 1. But the physical problems are associated with the known boundary conditions at the boundary points of irregular-shaped elastic bodies, which requires a further treatment to relate the values on the boundary with the field grid points. In this treatment a special technique is used to overcome this problem. In this context, the boundary of the problem is divided into four segments, namely, (i) the top-left, (ii) the bottom-left, (iii) the bottom-right and (iv) the top-right. These segments are then distinguished by selecting four points on the boundary of the elastic body. For designating any boundary point, a reference field grid point is used. For example, for a boundary point A in Fig. 1, the reference field grid point is P. If the boundary point matches with the field grid point, then the boundary point itself is the reference grid point, otherwise the reference grid points are selected in such a way that for a point on any boundary segment, the reference point is the nearest field grid point, immediately outside the boundary.

4.2. Transfer of boundary-values to grid-values (through interpolations)

The boundary value at the boundary point A would be approximately the linear interpolation of that of the four neighboring points P, Q, R and S, of Fig. 1. If the boundary points fall on the field grid point like point D it requires no interpolation. If it falls on the grid line like points B and C, then two points interpolation is required. Thus for a general case, for any boundary point, the boundary conditions involve a maximum of four field grid points of which one is reference point and it is always the nearest outside field grid point.

The boundary points are selected in such a way that for each boundary point, there must be a unique reference field

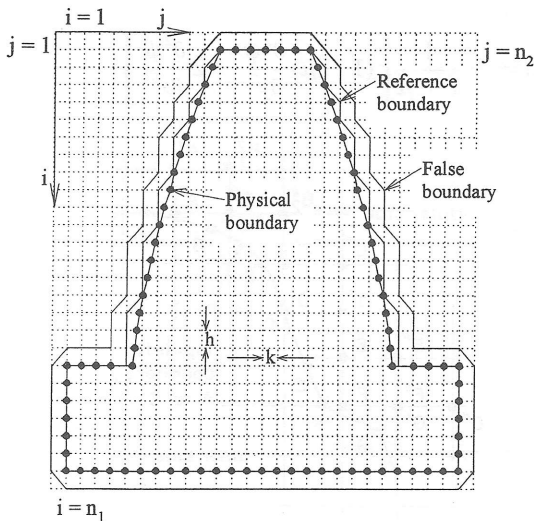


Fig. 6. Rectangular mesh-network used for the discretization of a typical gear tooth.

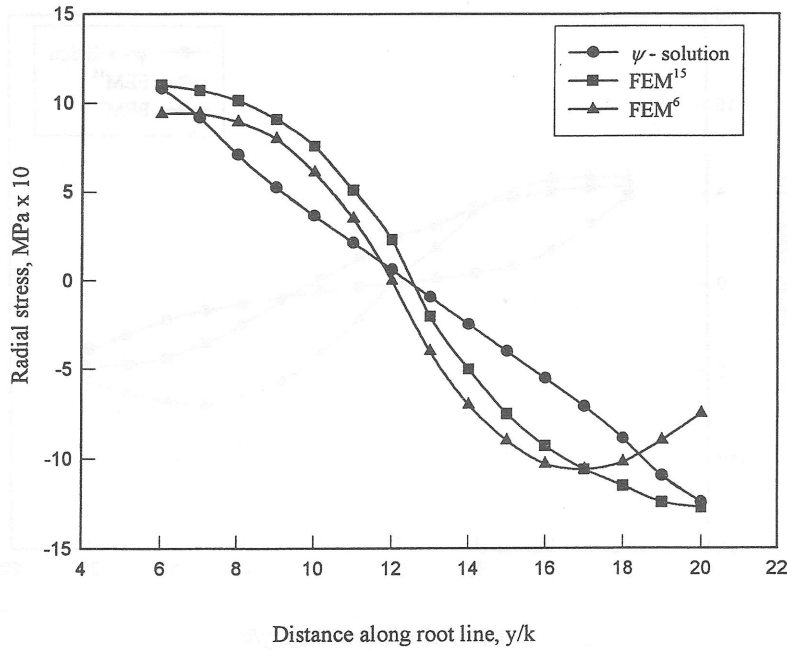


Fig. 7. Comparison of root stresses in gear tooth due to tip-loading.

grid point. Having decided upon the pattern and the total number of mesh points, we must provide a sufficient number of equations to solve for all the “discretized variables” (the values of the function at the mesh points) that result from the division of the domain into mesh points.

4.3. Matching of the nodal unknowns with the discretized algebraic equations

Considering an interior mesh point 1 (Fig. 1), it is seen

that the bi-harmonic equation in terms of ψ applied to this point will give rise to a single algebraic equation and therefore, the single unknown concerning this point has been provided with a single equation for its evaluation. Further, this algebraic equation will contain the discretized variable of the 13 neighboring mesh points from 1 to 13 in Fig. 1, provided all the derivatives present in the bi-harmonic equation are replaced by their respective central difference formulae. This implies that, when 1 becomes an immediate neighbor of the boundary, this equation will

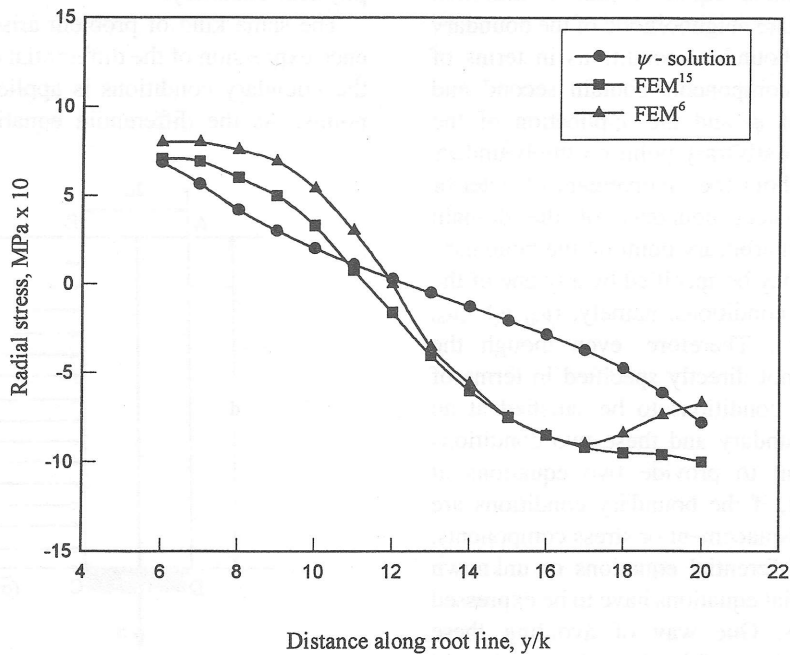


Fig. 8. Comparison of root stresses in gear tooth due to pitch-loading.

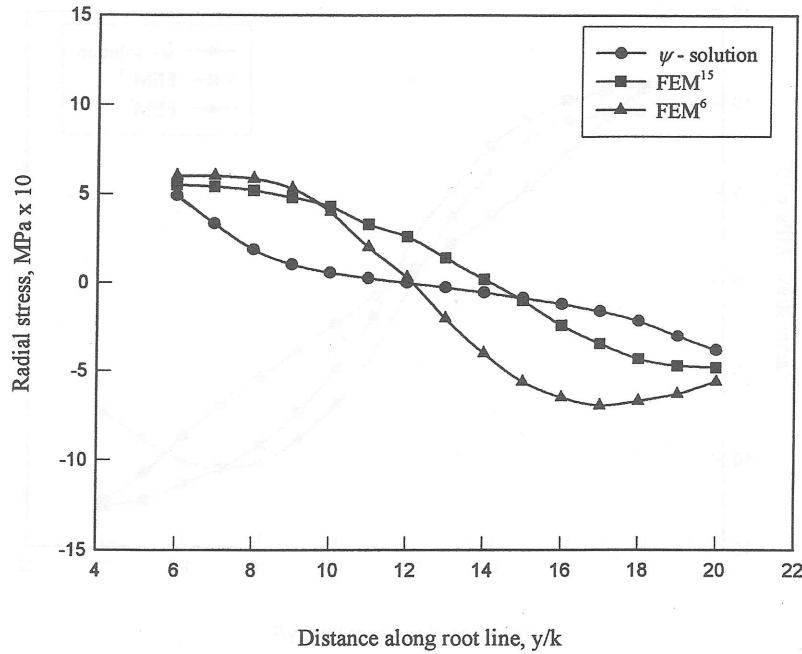


Fig. 9. Comparison of root stresses in gear tooth due to root-loading.

contain mesh points both interior and exterior to the boundary, as seen in Fig. 2. Among the exterior points some would be the reference grid points and the remainder would be extra points, other than the reference point. Thus, to match the discretized bi-harmonic equation with the domain of the field grid at least two exterior points should be considered. Thus, it is seen that, if the domain is discretized by lines parallel to the rectangular coordinate system then the application of the finite difference formulae of the bi-harmonic equation places limitation to the points in the immediate neighborhood of the boundary mesh points. Again, the boundary conditions in terms of stress and displacement components contain second and third order derivatives of ψ and the application of the boundary conditions at an arbitrary point on the boundary will not be very easy without the involvement of exterior mesh points to the physical boundary of the domain concerned. Considering an arbitrary point on the boundary, the boundary conditions may be specified by any one of the four groups of boundary conditions, namely, (u_n, u_t) ; (u_n, σ_t) ; (u_t, σ_n) or (σ_n, σ_t) . Therefore, even though the boundary conditions are not directly specified in terms of ψ , there are always two conditions to be satisfied at an arbitrary point on the boundary and these two conditions are theoretically sufficient to provide two equations at this point. In this respect, if the boundary conditions are given either in terms of displacement or stress components, that is, in the form of differential equations of unknown function ψ , these differential equations have to be expressed into difference equations. One way of avoiding these difficulties is by considering a false boundary with grid points exterior to the reference grid points of the domain

concerned. With this false boundary, the application of the central difference expressions of the bi-harmonic equation to the points in the immediate neighborhood of the physical boundary will cause no problem in the discretization of the domain. The new discretization of the domain with the false boundary mesh points in addition to its physical boundary is illustrated in the Fig. 2, showing the central differencing of the bi-harmonic equation applied to an arbitrary point in the immediate neighborhood of the physical boundary.

The same kind of problem arises when the finite difference expression of the differential equations associated with the boundary conditions is applied to the boundary mesh points. As the differential equations associated with the

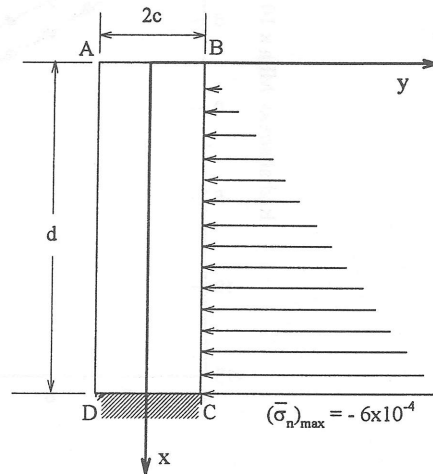


Fig. 10. Deep cantilever beam under hydrostatic loading.

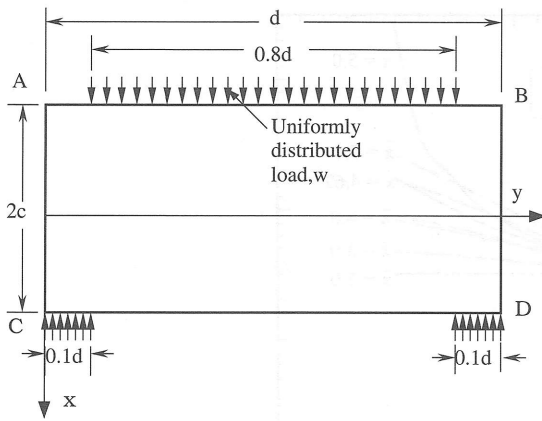


Fig. 11. Simply supported beam with uniformly distributed load.

boundary conditions contain second and third order derivatives of the function ψ , the application of the central difference expression is not practical as, most of the time, it may lead to the inclusion of the points exterior to the false boundary. One way of avoiding this problem is to replace the different first order derivatives of the function present in the boundary conditions by their two-point forward or backward difference formulae. The use of forward or backward difference formulae is dictated by the position of the mesh point on the boundary in order to avoid the occurrence of the mesh points external to the false boundary. But the local truncation error in this approach is of the order of h . A second way is to replace the above-mentioned derivatives in the boundary conditions by their three point forward or backward difference formulae. The local truncation error of this approach is of the order of h^2 . Theoretically, there is no problem in using any one of these two schemes in obtaining the finite difference expressions of the boundary conditions. But practical difficulty arises from the method of solution of the large number of algebraic equations obtained from the discretization of the governing differential equation and of the boundary conditions.

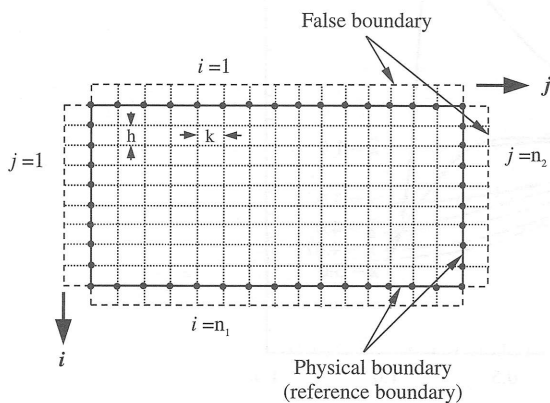


Fig. 12. Rectangular mesh-network used for the discretization of the beams.

4.4. Selection of physical boundary points with respect to field grid-points

In the application of the discretized formula of the bi-harmonic equation at any interior field grid point nearest to the boundary, it is seen that the structure of the formula demands at best two grid points on the grid line that passes through the concerned point. Out of these two grid points, the first one, closer to or on the boundary, is treated as the reference point and the second one, away from the boundary, is treated as the false boundary grid point. Since the body is arbitrarily bounded, the boundary points may not match with the field grid points (Fig. 1, point A). In this case, the physical boundary points are selected in such a way that for each boundary point there is one unique reference field grid point and for a continuous boundary the reference points are consecutive and without any repetition. To serve this purpose, the program is designed in such a fashion that the physical boundary points for each reference point R (Fig. 3) is the corresponding physical segment boundary point that lies on the intercepted boundary segment LN. Since, for the minimum number of boundary points, each boundary point should have a unique reference point, so for each reference point R, only one point L or M or N is selected as the boundary point at which the boundary condition is known. The reference point that lies on the boundary would be the corresponding boundary point.

4.5. Placement of boundary conditions

Since there are always two conditions to be satisfied at an arbitrary point on the physical boundary of the domain, the finite difference expressions of the differential equations associated with the boundary conditions are applied to the same point on the boundary. It leads to the fact that two linear algebraic equations are assigned to a single point on the boundary. The computer program is organized in such a fashion that out of these two equations, one is used to evaluate the reference point corresponding to the physical boundary point and the remaining one for the corresponding point on the false boundary and so on. Thus, every mesh point of the domain has a single linear algebraic equation and this system of algebraic equations will have to be solved by either direct or indirect methods of solution.

Another major problem is faced in formulating points on sharply turning boundary, like the corner point B, as seen in Fig. 4. Here, only the top-left portion of the whole boundary is shown. The points A, B, C, D, E, F & G on the physical boundary have the reference points A' , B' , C' , D' , E' , F' & G' , respectively. The reference points A' , B' , etc. are, of course, field grid points. For these reference points, the extra exterior grid points are A'' , $\{B_1'', B_2''\}$, C'' , D'' , E'' , F'' & G'' . For the geometry of the physical boundary point B there arise two exterior grid points B_1'' , B_2'' . Again for the boundary points like F & G, the extra grid point (F'') of F and reference point (G') of G may coincide at a point.

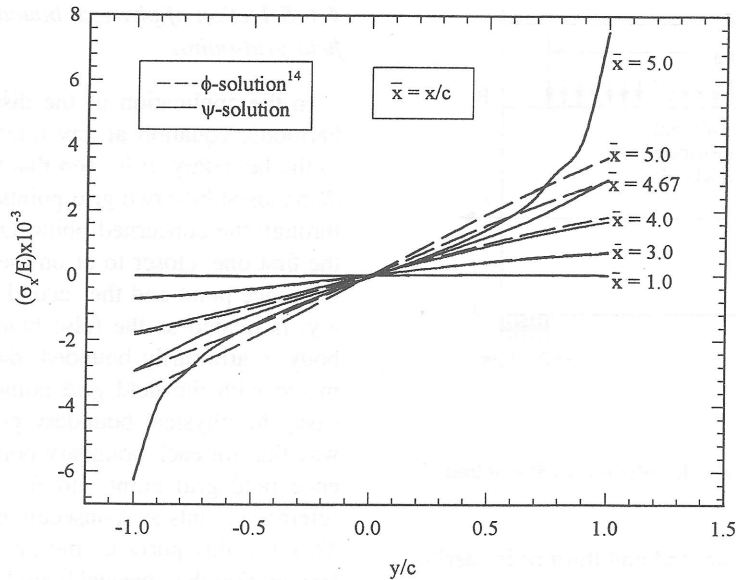


Fig. 13. Normalized bending stress distribution at different transverse sections of the deep cantilever beam, $d/c = 5$.

According to the earlier discussion, each boundary point has two boundary conditions; one is used for point of reference and other for the extended grid point. This scheme is satisfied by all the points except the points B and F or G. On the top-left boundary, there must be at least one point like B whose two extra exterior grid points are like B_1'' , B_2'' —one above and the other to the left of the reference point. For point B, only two boundary conditions are known but there arises three points, namely B' , B_1'' & B_2'' , leading to three unknowns. Thus, here, the number of unknowns exceeds the number of available equations. The problem can be resolved by using either (i) an additional boundary condition, or (ii) by assigning an arbitrary value of the unknown function ψ at

one of the three points, or (iii) omitting one of the two points (B_1'' , or B_2''). Here option (iii) is not practical because of the nature of finite difference equations associated with boundary conditions. Option (ii) is applicable for a maximum of three similar points. Because, the function ψ is a surface and if the surface (a) rotates as a whole or (b) translates as a whole or (c) tilts as a whole, the configuration of the surface remains unchanged, thus the desired results that depends only on the configuration of the surface remain the same. Option (i) can be satisfied by taking an additional boundary condition anywhere on the segment intercepted by the involved mesh boundary. The extra grid point (F'') of boundary point F and the reference point (G') for the

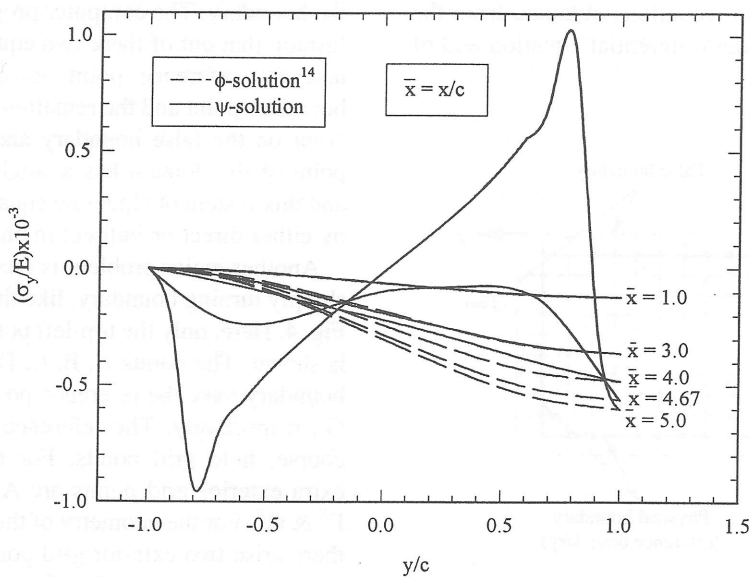


Fig. 14. Normalized transverse stress distribution at different transverse sections of the deep cantilever beam, $d/c = 5$.

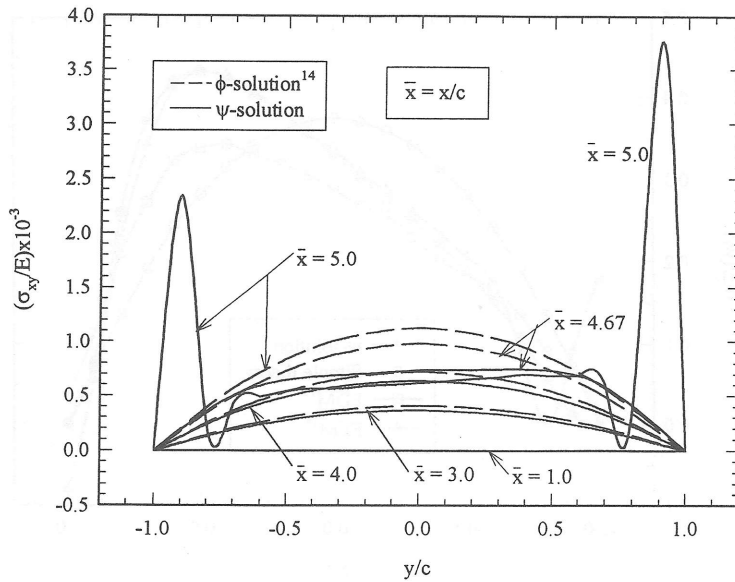


Fig. 15. Normalized shear stress distribution at different transverse sections of the deep cantilever beam, $d/c = 5$.

point G are coincident but have two boundary conditions, one from F and the other from G, that is, the number of unknowns is fewer than the number of conditions to be satisfied. One way to handle this sort of problem is to take the excess conditions as redundant.

5. Validation of the program

Using the above programming philosophy a FORTRAN code has been developed to handle regular as well as irregular-shaped elastic bodies for stress analysis. The code is available in Ref. [16]. It has been tested with some classical elastic problems like deep cantilevers

subjected to distributed transverse loading, deep cantilevers subjected to end shear, spur gear teeth with different loading, and short prismatic bars under tension and compression. The code is incorporated with zooming ability so that it can investigate details of stress-distribution over any critical region like discontinuities in boundary conditions, concentrated loading, and small notches. Here the results of spur gear teeth, deep cantilever subjected to hydrostatic loading, and simply supported deep beams with uniformly distributed load are presented in Figs. 7–9, Figs. 13–15 and Figs. 16–18, respectively, and compared with available results in the literature. In order to obtain the numerical results of these problems, values for Young’s modulus and Poisson’s ratio of 209 GPa and 0.3, respectively, are used.

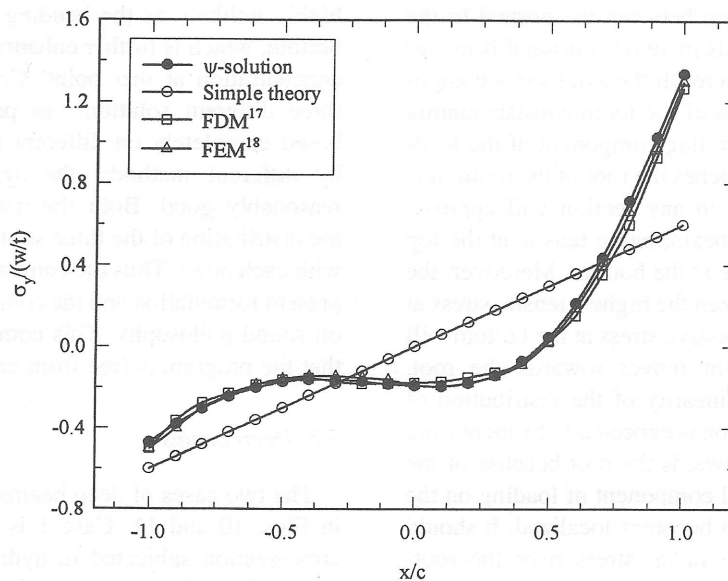


Fig. 16. Comparison of bending stress distributions at the mid-span of a simply supported, uniformly loaded deep beam ($d/c = 2$).

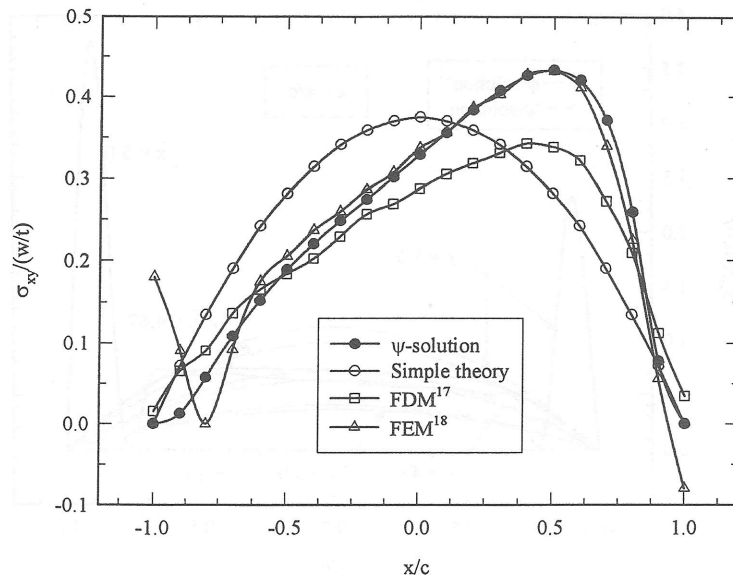


Fig. 17. Comparison of shear stress distributions at $y/d = 0.25$ in a simply supported, uniformly loaded deep beam ($d/c = 2$).

5.1. Spur gear tooth

The geometry of the gear tooth along with the boundary conditions are shown in Fig. 5. Fig. 6 shows the typical rectangular mesh network used for the discretization of the gear tooth domain.

The radial stress distributions at the root-section of the gear tooth (Fig. 5) due to tip, middle and root region loading are presented in Figs. 7–9. Also the results of the finite element method of the same problem, taken from Refs. [6,15], are plotted on the same graphs. The normal loading at the contact point on a gear tooth may be resolved into two components—one of axial compression and the other of bending. The compression component decreases gradually in magnitude as the contact point moves towards the root from the tip, because the angle between the normal to the tooth surface and the tooth-axis increases during this movement of the contact point. As a result the axial stress component on any transverse section of the tooth consists mainly of the stress caused by the bending component of the loading as the contact point approaches the root of the tooth. It is thus expected that stress σ_x on any section will approximately vary linearly, as in a beam, being tensile at the top (loaded side) and compressive at the bottom. Moreover, the difference in magnitude between the highest tensile stress at the top and the highest compressive stress at the bottom will decrease as the contact point moves towards the root. Further, the deviation from linearity of the distribution of axial stress over the root-section is expected to be increasing as the contact point moves towards the root because of the fact that the effect of the axial component of loading on the axial stress at the root-section becomes localized. It should be pointed out here that the radial stress over the root-section of the tooth, as shown in Figs. 7–9, is approximately the same as the axial stress in the x -direction in Fig. 5.

Keeping this in mind, as seen in Figs. 7–9, all the above contentions are met by the present solutions more closely than by the FEM solutions of Ref. [15] or of Ref. [6]. The deviation of the present solution from linearity is the least in Fig. 7 and increases gradually as the contact point moves towards the root, as seen in Figs. 8 and 9. The magnitude of maximum tensile stress at the root-section, as predicted by the present solution, is smaller than the magnitude of compressive stress at that section for the tip-loading but becomes gradually higher, as seen in Figs. 7 and 8, as the contact point moves towards the root, because of the increasing localized effect of loading. It should be pointed out here that the FEM solution of Ref. [6] predicts that the magnitude of the compressive stress at the bottom surface of the root-section is lower than that at points above it. This is highly unlikely as the bending stress is the highest at the bottom, which is further enhanced due to the effect of stress concentration at that point. Considering the fact that the three different solutions, as presented in Figs. 7–9, are based completely on different theories and found entirely by different methods, the agreement between them is reasonably good. Both the magnitude and the nature of the distribution of the three solutions are in good agreement with each other. Thus the comparative study verifies that the present formulation and the computer code are both founded on sound philosophy. This comparison establishes the fact that the program is free from errors and highly reliable.

5.2. Deep beams

The two cases of deep beams considered here are shown in Figs. 10 and 11. Case 1 is a cantilever of rectangular cross-section subjected to hydrostatic loading on its right vertical boundary, as shown in Fig. 10. Due to the lack of any reliable solution at the fixed support of such a deep

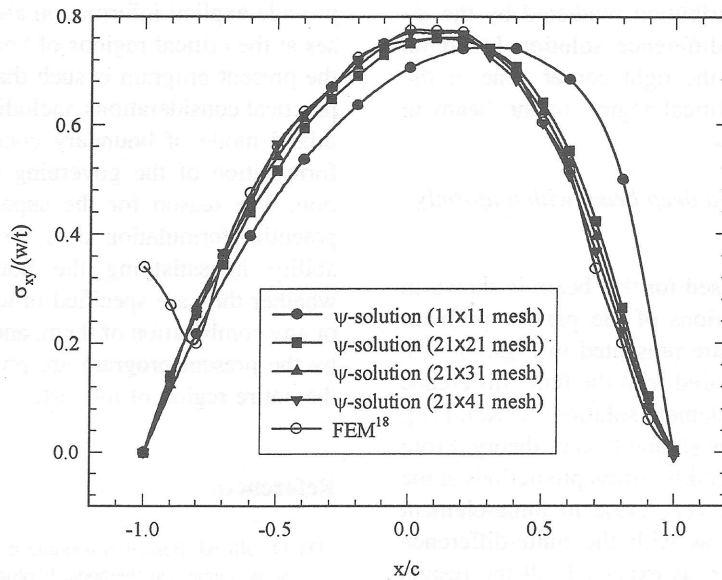


Fig. 18. Effect of grid size on the distribution of shearing stress at $y/d = 0.25$ in a simply supported, uniformly loaded deep beam ($d/c = 4$).

cantilever, our numerical solution is compared with the ϕ -solution given in Ref. [14]. Case-2 is a rectangular cross-section beam, which is simply supported at the ends and carries a uniformly distributed load over its free span. The extent of the supports and loading are chosen here to be identical to the model used by Chow et al. [17], and Hardy and Pipelzadeh [18] for analysis using the finite difference and finite element methods, respectively. The finite-difference mesh-network used for the discretization of the beams in relation to the coordinate system is presented in Fig. 12.

5.3. Case 1—deep cantilever subjected to hydrostatic loading

In the case of a deep cantilever subjected to hydrostatic loading, shown in Fig. 10, the boundary conditions, stated mathematically, are as follows: At the top edge, AB

$$\bar{\sigma}_n(\bar{x}, \bar{y}) = \bar{\sigma}_t(\bar{x}, \bar{y}) = 0 \quad \text{for } -1 \leq \bar{y} \leq 1, \bar{x} = 0 \quad (17)$$

At the left lateral edge, AD

$$\bar{\sigma}_n(\bar{x}, \bar{y}) = \bar{\sigma}_t(\bar{x}, \bar{y}) = 0 \quad \text{for } 0 \leq \bar{x} \leq 5, \bar{y} = -1 \quad (18)$$

At the bottom edge, DC, considered rigidly fixed

$$u_n(\bar{x}, \bar{y}) = u_t(\bar{x}, \bar{y}) = 0 \quad \text{for } -1 \leq \bar{y} \leq 1, \bar{x} = 5 \quad (19)$$

and at the right vertical edge, BC, for the hydrostatic loading

$$\bar{\sigma}_n(\bar{x}, \bar{y}) = -(qc/E)\bar{x}, \quad \text{and } \bar{\sigma}_t(\bar{x}, \bar{y}) = 0 \quad (20)$$

for $0 \leq \bar{x} \leq 5, \bar{y} = 1$

where, c is the half depth of the beam, q is the specific weight of the liquid, the variables, $\bar{x} = x/c, \bar{y} = y/c$, and the constant, $(qc/E) = 1.2 \times 10^{-4}$. For this problem, the

analytical solution of Ref. [14] is

$$\bar{\sigma}_x = \frac{qc\bar{x}}{E} \left\{ \frac{\bar{x}^2\bar{y}}{4} - \frac{\bar{y}^3}{2} + \frac{3\bar{y}}{10} \right\} \quad (21)$$

$$\bar{\sigma}_y = \frac{qc\bar{x}}{E} \left[\frac{-1}{2} + \frac{\bar{y}^3}{4} - \frac{3\bar{y}}{4} \right] \quad (22)$$

$$\bar{\sigma}_{xy} = \frac{qc\bar{x}}{E} \left[\frac{3}{8}(\bar{x} - \bar{x}\bar{y}^2) - \frac{1}{8} \left(\frac{1}{\bar{x}} - \frac{\bar{y}^4}{\bar{x}} \right) + \frac{3}{20} \left(\frac{1}{\bar{x}} - \frac{\bar{y}^2}{\bar{x}} \right) \right] \quad (23)$$

The analytical solution does not satisfy the boundary conditions at the bottom edge. So, the two solutions are expected to differ as \bar{x} increases. Fig. 13 shows the comparison of σ_x found by the present program with that found by the ϕ -solution in Ref. [14]. The comparison shows that the two results are very close to each other for smaller \bar{x} and differ appreciably as \bar{x} approaches the bottom edge, conforming fully to our expectation. The results of σ_y and σ_{xy} in Figs. 14 and 15, respectively, compare very well with the results of Ref. [14], except near the fixed edge, as expected. The deviations in the results found for σ_y and σ_{xy} near the fixed end are due to the difference in boundary management of the two methods, the present method accounting for it fully while the ϕ -solution only partially. It should be noted here that, for this cantilever beam, the magnitude of $\bar{\sigma}_x$ at the right corner (loaded side) of the fixed support is found to be higher than that at the left corner; however, in the case of ϕ -solution this magnitude is exactly the same for both corners (Fig. 13). Similarly, the distribution of shearing stress, as shown in Fig. 15, predicted by our ψ -solution reveals that the actual distribution at the fixed support differs significantly in magnitude as well as in shape

from the usual parabolic distribution predicted by the ϕ -solution. The present finite-difference solution based on our ψ -formulation identifies the right corner zone of the fixed support as the most critical region in the beam in terms of stresses.

5.4. Case 2—simply supported deep beam with uniformly distributed load

The boundary conditions used for this beam is shown in Fig. 11. The numerical solutions of the present problem based on our ψ -formulation are presented in Figs. 16–18, where the solutions are compared with the finite-difference solutions of Ref. [17], finite-element solutions of Ref. [18], and also with that predicted by simple flexure theory. From Fig. 16, we can see that our bending stress predictions at the mid-section of the beam are very close to finite-element results of Ref. [18] as well as with the finite-difference results of Ref. [17]. However, as expected, all the results differ significantly from that predicted by the simple theory. Again as appears from the shearing stress distribution over the depth at section, $y/d = 0.25$, shown in Fig. 17, the present finite-difference solution agrees well with the finite element predictions; both the solutions predict nearly identical maximum shearing stress at the same position of the section, which is, however, observed to be approximately 26% higher than that predicted by the finite-difference results of Ref. [17]. This is because of the obvious inaccuracies in the finite-difference method of Ref. [17], where a 6×6 mesh network had been used. Another interesting observation from the figure is that the finite element method of solution fails to predict the actual state of the stress at the boundaries, even though the section concerned is free from singularity; however, our present numerical model is capable of predicting the state of stresses accurately at the boundary as well as within the body.

Finally, the effect of mesh size on the present numerical solution is illustrated in Fig. 18. Here the distribution of shearing stress at section $y/d = 0.25$ of the simply supported deep beam of $d/c = 4$ is shown. From the distribution, it is observed that, when a coarse mesh network (large grid size) is used to discretize the domain, the result is observed to deviate substantially from that of finer mesh results. This is because of the fact that the error of the present computational approach is of the order of h^2 . Therefore, generally, as the grid size decreases, error decreases quadratically with the mesh size h . Hence, no significant change in the distribution is observed with decreasing h when it is sufficiently small, as confirmed by the results here.

6. Conclusions

Earlier mathematical models of elasticity were very deficient in handling practical problems. No appropriate approach was available in the literature, which could

provide explicit information about the distribution of stresses at the critical regions of boundaries. The philosophy of the present program is such that it encompasses all sort of practical considerations, including sharp discontinuities and mixed mode of boundary conditions with an appropriate formulation of the governing equations—the ψ formulation. The reason for the superiority of the displacement potential formulation over the existing approaches is its ability in satisfying the boundary conditions exactly, whether they are specified in terms of loading or restraints or any combination of them, and thus the solutions obtained by the present program are promising and satisfactory for the entire region of interest.

References

- [1] Durelli AJ, Ranganayakamma B. On the use of photo elasticity and some numerical methods. *Photomechanics and Speckle Metrology*, SPIE 1987;814:1–8.
- [2] Durelli AJ, Ranganayakamma B. Parametric solution of stresses in beams. *Journal of Engineering Mechanics* 1989;115(2):401.
- [3] Chong TH, Suzuki T, Kubo A, Fujio H. Tooth fillet stresses of gear with thin rim. *Bulletin of the JSME* 1983;26:1799–806.
- [4] Andrews JD. A finite element analysis of bending stress induced in external and internal spur gears. *Journal of Strain Analysis* 1991;26(3):153–63.
- [5] Sayama T, Oda S, Umezawa K, Makuta H. Study on welded structure gears. *Bulletin of the JSME* 1984;27:1763–72.
- [6] Ramamurti V, Nayak HV, Sujatha C. Static and dynamic analysis of spur and bevel gears using FEM. *Advances in mechanical engineering*. New Delhi: Narosa Publishing-House, 1996. p. 1291–313.
- [7] Airy GB. *British Association for the Advancement of Science Rept.* 1862.
- [8] Uddin MW. Finite difference solution of two-dimensional elastic problems with mixed boundary conditions. MSc Thesis, Carleton University, Canada, 1966.
- [9] Dow JO, Jones MS, Harwood SA. A new approach to boundary modeling for finite difference applications in solid mechanics. *International Journal for Numerical Methods in Engineering* 1990;30:99–113.
- [10] Idris ABM. A new approach to solution of mixed boundary value elastic problems. MSc Thesis, Bangladesh University of Engineering and Technology, Bangladesh, 1993.
- [11] Ahmed SR, Khan MR, Islam KMS, Uddin MW. Analysis of stresses in deep beams using displacement potential function. *Journal of Institution of Engineers (India)* 1996;77:141–7.
- [12] Ahmed SR. Numerical solutions of mixed boundary-value elastic problems. MSc Thesis, Bangladesh University of Engineering and Technology, Bangladesh, 1993.
- [13] Horgan CO, Knowles JK. Recent development concerning Saint-Venant's principle. *Advances in Applied Mechanics* 1983;23:179–269.
- [14] Timoshenko S, Goodier JN. *Theory of elasticity*, 3. New York: McGraw-Hill, 1979.
- [15] Ramamurti V, Rao MA. Dynamic analysis of spur gear teeth. *Computers and Structures* 1988;29(5):831–43.
- [16] Akanda MAS. Stress analysis of gear teeth. MSc Thesis, Bangladesh University of Engineering & Technology, Bangladesh, 1997.
- [17] Chow L, Conway HD, Winter G. Stresses in deep beams. *Transactions of the American Society for Civil Engineers*, paper no. 2557, 1952.
- [18] Hardy SJ, Pipelzadeh MK. Static analysis of short beams. *Journal of Strain Analysis* 1991;26(1):15–29.